RSC Advances

ROYAL SOCIETY OF CHEMISTRY

www.rsc.org/advances

Table of Contents Entry

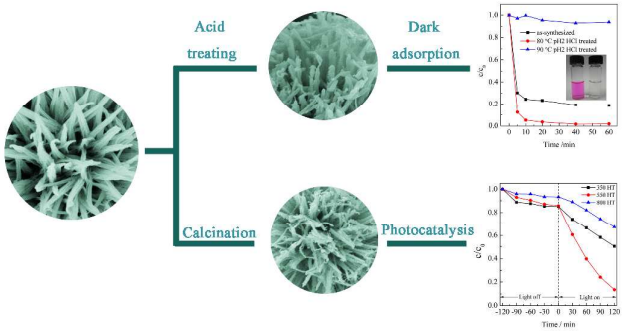

Hierarchical flower-like $H_2Ti_5O_{11}\cdot 3H_2O$ assembled with radial nanowires was fabricated through a template-free solution-based method, which could be converted to TiO_2 with controllable morphologies and phased by a subsequent acid-treating or annealing process.

Cite this: DOI: 10.1039/c0xx00000x

www.rsc.org/xxxxxx

ARTICLE TYPE

A facile synthesis of hierarchical TiO_2 for dye adsorption and photocatalysis

Lu-Lu Lai[a] and Jin-Ming Wu*[a]

Received (in XXX, XXX) Xth XXXXXXXXX 20XX, Accepted Xth XXXXXXXXX 20XX

DOI: 10.1039/b000000x

Hierarchical flower-like $H_2Ti_5O_{11}·3H_2O$ assembled with radial nanowires was fabricated via a template-free solution-based reaction, which was converted to TiO_2 with distinct phases and morphologies by the subsequent acid-treating or annealing. The HCl treatment achieved the controllable conversion from titanate nanowires to rutile nanorods by varying the temperature and acidity. When compared with the as-synthesized titanate nanowires and the thoroughly transformed rutile nanorods, their mixtures were found to exhibit the best dye adsorption ability towards rhodamine B and methylene blue in water. The $H_2Ti_5O_{11}·3H_2O$ nanowires decomposed in sequence to anatase and rutile after a subsequent calcination in air, via an intermediate phase of $H_2Ti_4O_9·H_2O$. The hierarchical structure could be retained for up to 800 ^oC. When utilized as photocatalysts to degrade rhodamine B in water, the 550 ^oC-calcinated powder, with mixed phases of anatase, rutile, and srilankite, demonstrated the highest photocatalytic activity.

Introduction

Titania (TiO_2) is an important semiconductor finding wide applications in fields of photocatalysts,[1] dye-sensitized solar cells (DSSCs),[2] Li-ion batteries,[3] gas sensors,[4] photoelectrochemical devices,[5] and so forth. It is exhaustively explored for the merits of environmental friendliness, chemical inertness, high stability, non-toxicity, and low cost, when utilized as photocatalysts for environmental remediation.[6] Nanostructured titania, especially that with hierarchical nanostructures, have drawn increasing attention owing to their unique and fantastic properties.[7] Given that three dimensional (3D) nanostructures possess larger specific surface area and abundant active sites, so far many 3D titania hierarchical structures have been reported, such as hierarchical nanowires,[8] hierarchical nanotubes,[9] nanoboxes,[10] nanocages,[11] polyhedra,[12] and microspheres.[4,13-20] The most popular amongst the various kinds of 3D hierarchical nanostructures are hierarchical microspheres with diverse building blocks, for instance, nanoflakes,[4] nanosheets,[13,14] nanoribbons,[15] nanobelts,[16] nanopetals,[17] nanoneedles,[18] nanorods,[19] and nanowires.[20]

Several methods have been developed to synthesize 3D hierarchical structures, including hydrothermal, sol-gel, and hydrolysis procedures. Up to now, most of these works utilize hydrothermal or solvothermal approaches, which are energy-consuming as a result of the high reaction temperature, and require high pressure apparatus. The starting materials often involve titanium isopropoxide (TTIP), tetrabutyl titanate (TBOT), and $TiCl_4$, which are difficult to handle with.[21] Only limited researches adopt a non-hydrothermal route to prepare titania with 3D hierarchical structures. Dou et al. synthesized titania hierarchical architecture, including nanospheres, microspheres, and cauliflowers, through a facile hydrolysis process of $TiCl_4$ combining with the induction of pollen.[22] Tsai et al. fabricated titania nanocages by a sol-gel procedure with the assistance of NaF cubic templates.[11]

In this work, we report a non-hydrothermal and template-free synthesis of a hierarchical titania by a direct reaction between metallic Ti powders and hydrogen peroxide solution at 80 ^oC. Hydrogen titanate nanowires were achieved directly, assembling to form a 3D flower-like hierarchical structure. Transformations of the hydrogen titanate to titania were studied in detail by a subsequent HCl treatment or calcination in air. The performance for the resultant 3D titania powders as both dye absorbents and photocatalysts for dye degradations were evaluated, which is in related to the structural evolutions.

Experimental section

Synthesis

In a beaker, 90 mg of metal Ti powders (200 mesh) were added to 300 mL 30 wt. % H_2O_2 aqueous solution which contained HNO_3 (0.29 M) and melamine (2.4 mM). Bath sonication was carried out for 10 min. Subsequently, the beaker was sealed and placed in an oven maintained at 80 ^oC for 48 h. The precipitates were collected by centrifugation, washed in sequence with deionized water and ethanol for three times, and dried in air at 80 ^oC overnight. For the HCl treatment, 62.5 mg of the as-synthesized powders were immersed in 250 mL HCl aqueous solution with pH values of 1.5 (0.03 M) and 2.0 (0.01 M), at temperatures of 80 and 90 ^oC, respectively. The calcination was carried out in air at 250, 350, 550, and 800 ^oC for 1 h.

Characterization

The morphologies were examined by a field emission scanning

electron microscopy (FESEM, Hitachi, S-4800). The X-ray diffraction (XRD) tests were performed using a Rigaku D/max-3B diffractometer with CuKα radiation, operated at 40 kV, 36 mA (λ= 0.15406 nm). A DSCQ1000 instrument (Waters) was used to carry out the thermogravimetric (TG) and differential scanning calorimetry (DSC) investigations of the as-synthesized powders in an air atmosphere at a heating rate of 10 K min^{-1} from room temperature to 850 ^{o}C. Fourier transform infrared spectra (FT-IR) were recorded with the KBr pellet technique in the range of 4000—400 cm^{-1} on a Nicolet 5700 infrared spectrophotometer (ThermoFisher Co. Ltd.). The Brunauer-Emmett-Teller (BET) approach using adsorption data was utilized to determine the specific surface area. The sample was degassed at 80 ^{o}C for 25 h to remove physisorbed gases prior to the measurement.

Adsorption experiment

The adsorption performance of the as-synthesized powders and those after HCl treatments (pH2.0, 80 ^{o}C and 90 ^{o}C for 72 h) was evaluated using rhodamine B (RhB), methylene blue (MB), and methyl orange (MO) in water, respectively. All the experiments were carried out under a vigorous stirring in dark at room temperature. 25 mg of the powders were added into 50 mL solutions of RhB, MB and MO, respectively, with initial concentrations of 4.8 mg/L, 20 mg/L and 17.5 mg/L. At certain intervals, an appropriate amount of the suspension was taken out and centrifuged. The dye concentration was determined with a UV-Vis spectrophotometer (UV-1800PC, Shanghai Mapada Instruments Co. Ltd, Shanghai, China) at the wavelength of 553, 664, and 464 nm for RhB, MB and MO, respectively, after removing the powders by centrifugations. To investigate the adsorption capacity under an acidic environment, the dye solution was adjusted to pH4 using concentrated HCl solution.

Photocatalytic test

The photocatalytic performance of the calcinated powders was evaluated via photodegradation of RhB in water. 25 mg powders were dispersed into 50 mL RhB solution with an initial concentration of 4.8 mg/L, which was firstly stirred in dark for 120 min to reach an adsorption-desorption equilibrium and then subject to a UV-lamp irradiation for additional 120 min. The average intensity of UV irradiance reaching the sample was 5.0 mW cm^{-2}, measured for the wavelength range of 320—400 nm with a peak wavelength of 365 nm (Model: UV-A, Beijing Normal University, China). The change in RhB concentration was monitored as described in the adsorption experiment.

Results and Discussion

HCl-induced transformation and dye adsorption

Hierarchical flower-like nanostructures assembled with nanowires with an average length of 1 μm and a length/diameter ratio of ca. 25~40, as displayed in **Fig. 1**a, b, was fabricated by the present facile non-hydrothermal and template-free approach. The XRD pattern demonstrated in **Fig. 2**a suggests that the as-synthesized powders are hydrogen titanate of pentatitanate $H_2Ti_5O_{11}{\cdot}3H_2O$ (JCPDS card 44-0130). After the HCl treatment, nanowires changed to nanorods with an average length/diameter ratio estimated to be ca. 15~20, which also assembled to give a flower-like appearance (**Fig. 1**c-f). When treated at 80 ^{o}C, rutile phase coexisted with the original protonated pentatitanate (**Fig. 2**b, c). The XRD intensity for the peak located at 8.4 ^{o} in 2θ, which is the strongest XRD peak for the protonated pentatitanate, decreased significantly with increasing HCl concentration. All the XRD peaks corresponding to protonated pentatitanate diminished after the HCl treatment at 90 ^{o}C for 72 h, for which rutile was detected, together with trace anatase (**Fig. 2**d, e).

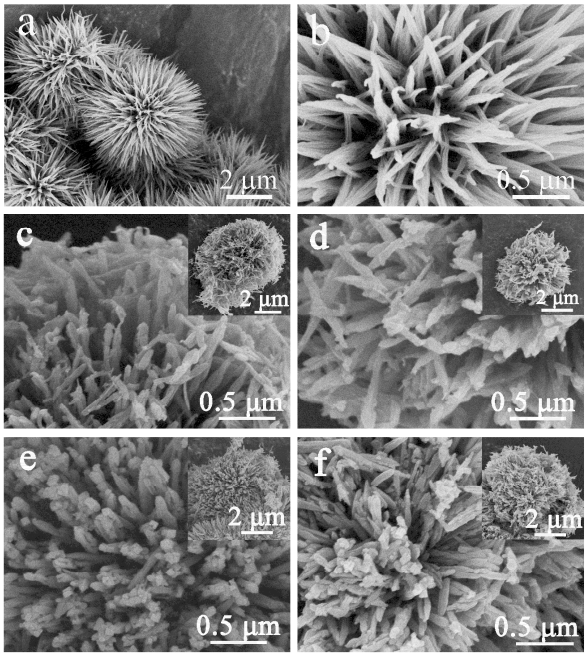

Fig. 1 FESEM images of (a, b) the as-synthesized powders and those after HCl treatments for 72 h: (c) pH2.0, 80 ^{o}C; (d) pH1.5, 80 ^{o}C; (e) pH2.0, 90 ^{o}C; (f) pH1.5, 90 ^{o}C.

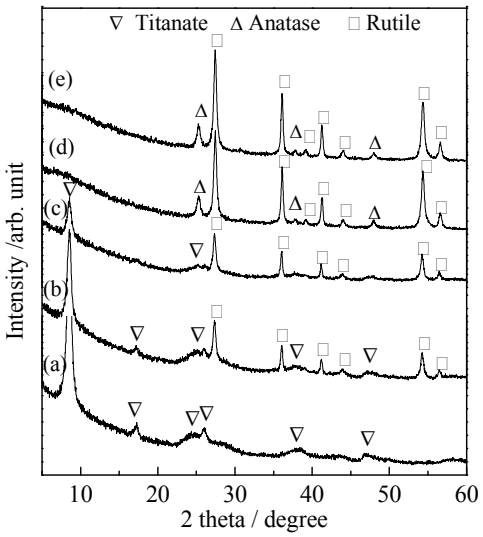

Fig. 2 XRD patterns of (a) the as-synthesized powders and those after HCl treatments for 72 h: (b) pH2.0, 80 ^{o}C; (c) pH1.5, 80 ^{o}C; (d) pH2.0, 90 ^{o}C; (e) pH1.5, 90 ^{o}C.

The morphological change from nanowires to nanorods suggests a dissolution precipitation procedure during the HCl treatment. The protonated pentatitanate nanowires gradually

dissolved and released Ti(IV) ions into the HCl solution. Because of the limited solubility of Ti(IV) ions in water, hydrated Ti(IV) ions saturated easily and tiny rutile nanocrystals were supposed to precipitate, which further assembled into rutile nanorods. The selective adsorption of Cl^- ions, as well as an acidic environment, favored the formation of rutile nanorods.[23] The transformation from hydrogen titanate nanowires to titania nanorods was incomplete when treated at 80 ºC, which can find support also from the remained nanowires in **Fig. 1**c, d. The dissolution precipitation procedure was remarkably accelerated by the increasing temperature and HCl concentration.

Figure 3 shows the low temperature (77 K) nitrogen adsorption-desorption isotherms of the as-synthesized powders, and those subjected to the pH2 HCl treatment at 80 °C and 90 °C. The specific surface area of the as-synthesized powders was 60.6 $m^2 \cdot g^{-1}$. The part transformation of hydrogen titanate nanowires to rutile nanorods in pH2 HCl at 80 °C reduced slightly the specific surface area to ca. 52.2 $m^2 \cdot g^{-1}$. The largest specific surface area of ca. 92.0 $m^2 \cdot g^{-1}$ is achieved for the powders treated with pH2 HCl at 90 °C for 72 h, which may be attributed to the increasing amounts of anatase nanoparticles (comparing **Fig. 2**b and d).

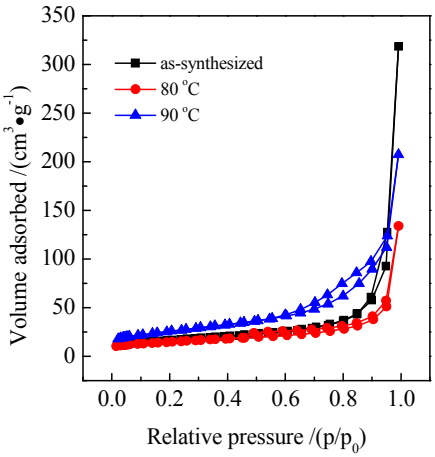

Fig. 3 The N_2 adsorption-desorption isotherms of the as-synthesized powders, and those after pH2.0 HCl treatments for 72 h at 80 °C and 90 °C.

Dye adsorptions by absorbents of oxides or titanates are interesting topics for efficient treatments of dye effluents.[24,25] The as-synthesized powders and those after treating with pH2 HCl at 80 °C and 90 °C for 72 h were subjected to dye adsorption tests. **Fig. 4**a, c demonstrates that, the powders treated with pH2 HCl at 80 °C for 72 h absorbed 95% RhB within 10 min and 63% MB within 40 min (note the difference in the initial concentration). For each dye molecule of RhB or MB, the as-synthesized powders exhibited decreased removal efficiency; whilst the powders treated with pH2 HCl at 90 °C for 72 h possessed negligible adsorption capacity. MO molecules can hardly be adsorbed by all the three powders (**Fig. 4**e). Industrial dye effluents are commonly in an acidic state. **Fig. 4**b, d, f illustrates a similar trend in the adsorption capacity for dye molecules under an acidic environment of pH4.0.

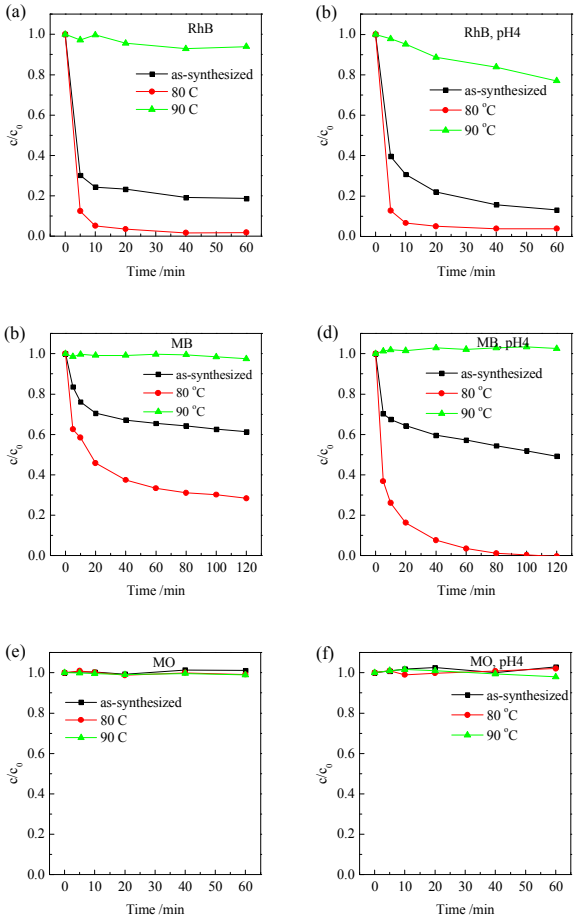

Fig. 4 Dark adsorption of (a, b) RhB, (c, d) MB, and (e, f) MO in water in the presence of the as-synthesized powders, and those after pH2.0 HCl treatments for 72 h at 80 °C and 90 °C. (b, d, f) the corresponding dye molecules in the pH4 environment.

The adsorption capacity of the as-synthesized powders can be attributed to the interspace surface of the layered titanate and the electrostatic attraction. Feng *et al.* fabricated hierarchical flower-like sodium titanate and reported significant removal towards MB but negligible adsorption towards RhB.[25] The results were attributed to the fact that RhB possesses a bigger molecule size than MB. In the current investigation, for the as-synthesized powder and that subjected to the pH2 HCl treatment at 80 °C for 72 h, the dye adsorption capacity towards RhB is also remarkable. This might be attributed to the larger interlayer spacing of the present $H_2Ti_5O_{11} \cdot 3H_2O$ titanate nanowires (1.04 nm[26] vs. 0.92 nm[25]), which alleviated the size limitation.

The total disappearance of the layered titanate, when treated by HCl at 90 °C, resulted in the negligible dye adsorption capacity towards RhB, MB and MO. However, when treated at 80 °C, which induced partial transformation of the layered titanate to rutile nanorods, the dye adsorption capacity towards RhB and MB increased significantly. The further enhanced dye adsorption cannot be attributed to the change in the specific surface area because the total transformation of the 90 °C-treated titanate nanowires resulted in negligible dye adsorption capacity; whilst the specific surface area is even larger than those treated at 80 °C (**Fig. 3**). The low temperature precipitated rutile nanorods

have been confirmed to possess abundant surface hydroxyl groups.[23] Such negatively charged rutile contacted closely with the unchanged layered titanate (**Fig. 2**c), which is thus assumed to work together to give a further enhanced dye adsorption capacity towards RhB and MB, both of which are positively charged in water. For the negatively charged MO molecules, no adsorption can be observed for all the powders, which is in good accordance with Feng et al.[25]

Calcination-induced transformation and photocatalysis

Figure 5 indicates the TG-DSC curve of the as-synthesized $H_2Ti_5O_{11}\cdot 3H_2O$ powders. The thermal decomposition procedure can be divided into three stages judging from the weight loss: stage I, a gradual weight loss of 7.3 wt. % in the temperature range from room temperature to 250 °C with a broad endothermic peak; stage II, a rapid weight loss of 17.0 wt. % in the temperature range 250–350 °C accompanying a sharp exothermic peak; stage III, a gradual weight loss of 4.7 wt. % in the temperature range 350–800 °C with a small broad exothermic peak.

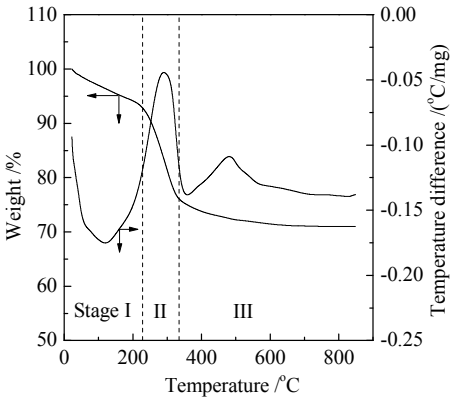

Fig. 5 TG and DSC curves of the as-synthesized powders recorded in air atmosphere at a 10 K/min heating rate.

To determine the ascriptions of the three DSC peaks, the as-synthesized powders were subjected to calcination in air at several crucial transition temperatures and the XRD patterns were measured and illustrated in **Fig. 6**. $H_2Ti_5O_{11}\cdot 3H_2O$ possess a structure in which six water molecules are accommodated in a unit interlayer space encircled by a pair of the block $[Ti_{10}O_{22}]^{4-}$.[26] An intermediate hydrogen titanate $H_2Ti_4O_9\cdot H_2O$ (JCPDS card 36-0655) was obtained after heating at 250 °C for 1 h (**Fig. 6**b). It is assumed that this transformation was accomplished by losing the free interlayer water molecules and the adjustment of the block from $[Ti_{10}O_{22}]^{4-}$ to $[Ti_8O_{18}]^{4-}$.[26] **Fig. 6**c shows that, further increasing the calcination temperature to 350 °C led to the decomposition of the intermediate $H_2Ti_4O_9\cdot H_2O$ phase to anatase and srilankite (JCPDS card 21-1236), which resulted in the sharp exothermic peak during stage II as demonstrated in **Fig. 5**. For the temperature above 350 °C, the phase transformation of TiO_2 from anatase and/or srilankite to rutile took place, bringing about the exothermic peak in stage III in **Fig. 5**. At 550 °C, a mixed phase of anatase, srilankite and rutile was achieved. Phase pure rutile with high crystallinity was obtained when the calcination temperature reached 800 °C (**Fig. 6**e).

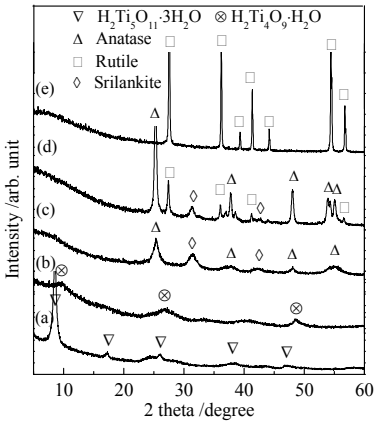

Fig. 6 XRD patterns of the as-synthesized powders (a) and those after calcination at various temperatures for 1 h (b) 250 °C; (c) 350 °C; (d) 550 °C; (e) 800 °C.

The FT-IR spectra of the as-synthesized powders and those subjected to calcination at 550 °C were shown in **Fig. 7**. For the as-synthesized powders, the bands between 500 and 950 cm^{-1} can be attributed to the Ti-O-Ti vibration, and the vibration of absorbed water molecules is found at 3000–3600 cm^{-1} and 1660 cm^{-1}.[27] The bands between 1000 and 1300 cm^{-1} are attributed to the Ti-OH vibration, within which bands at 991 cm^{-1} and 1086 cm^{-1} can be discerned.[28] The sharp band at 1730 cm^{-1} originates from the vibration of C=O.[29] Moreover, the bands between 1400 cm^{-1} and 1650 cm^{-1} are generated from triazine vibrations (**Fig. 7**a).[30] These results demonstrate that the as-synthesized powders contain reactant melamine and its hydrolysis products. After calcination at 550 °C, the vibrations related to triazine and C=O disappeared, revealing the complete decomposition of melamine and other impurities. The bands located at 1639 cm^{-1} and 3435 cm^{-1} can still be discerned, which can be attributed to the vibration of water molecules absorbed from the environment moisture. Besides, the band at 1083 cm^{-1} corresponding to Ti-OH vibration can also be found for the powders calcinated at 550 °C.

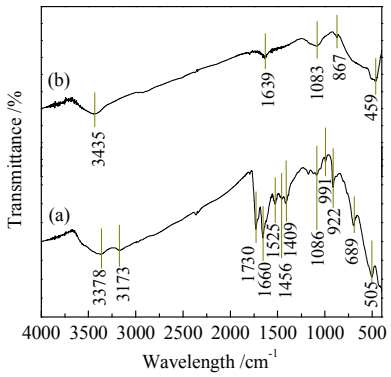

Fig. 7 FT-IR spectra of the as-synthesized powders (a) and those after calcination at 550 °C for 1 h (b).

The reactions in correspond to stage I and II can be formulated as follows:

$$4H_2Ti_5O_{11}\cdot 3H_2O \rightarrow 5H_2Ti_4O_9\cdot H_2O + 6H_2O \quad \text{Eq. (1)}$$

$$H_2Ti_4O_9 \cdot H_2O \rightarrow 4TiO_2 + 2H_2O \quad \text{Eq. (2)}$$

The measured weight loss in stage I (7.3 wt. %) and stage II (17 wt. %), respectively, is larger than the theoretic values of 5.7 wt. % and 10.1 wt. % according to Eq. (1) and Eq. (2). This can be attributed to the organic impurities resulted from melamine in H_2O_2 solution, as well as additional water molecules absorbed, as revealed in **Fig. 7**a. The absorbed water molecules gradually desorbed and the organic decomposition occurred during the whole heating procedure.[31]

The hierarchical flower-like structure assembled by nanowires fabricated in the current investigation can be well maintained as the calcination temperature increases to 550 °C; however, nanowires became rough in appearance (**Fig. 8**b). Further increasing the temperature to 800 °C, the hierarchical structure can still be well preserved while the building blocks changes from nanowires to a nanolotus-like structure (**Fig. 8**c, d).

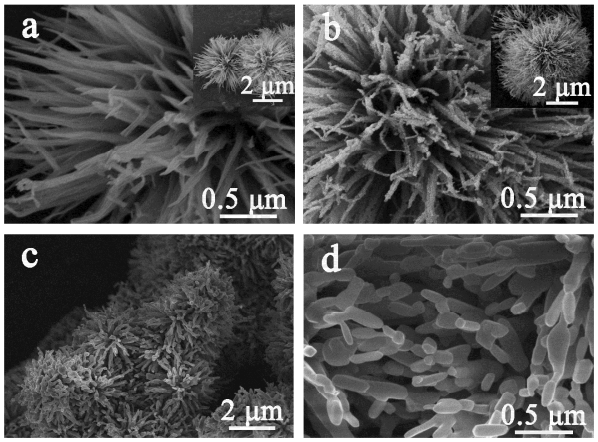

Fig. 8 FESEM images of the powders calcinated for 1 h at (a) 350 °C, (b) 550 °C and (c, d) 800 °C.

The calcinated powders were employed to assist photodegradation of rhodamine B in water under UV illumination (**Fig. 9**). Under the irradiation of UV light, electrons in the valence band of titania are excited to the conduction band, creating electron-hole pairs, which migrate to surface to be involved in the photocatalytic reaction. The highly oxidative surface holes can induce directly the degradation of RhB molecules. Also, the photogenerated holes and electrons can be trapped by surface hydroxyl groups and oxygen to form hydroxyl radicals and oxygen species, respectively, which further oxide RhB molecules to carbon dioxide, water and mineral acids.[32]

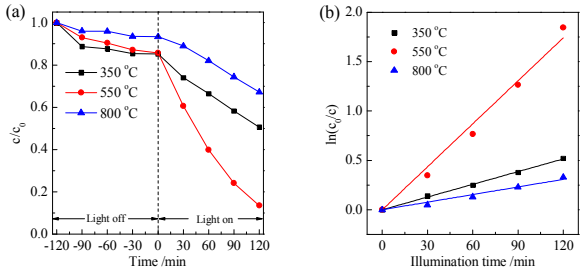

Fig. 9 (a) Photodegradation of rhodamine B in water in the presence of the powders calcinated for 1 h at 350 °C, 550 °C and 800 °C. The fitting results assuming a pseudo-first order reaction were presented in (b).

Figure 9 illustrates that, the 800 °C-calcinated powder exhibited negligible adsorption within the 120 min dark adsorption; while the powders calcinated at 350 and 550 °C adsorbed *ca.* 15 % rhodamine B molecules. The 550 °C-calcinated powders demonstrated the best photocatalytic activity by decomposing more than 90 % rhodamine B within 120 min. The photodegradation process can be well fitted into a pseudo-first order reaction (**Fig. 9**b). The reaction rate constant for the 550 °C-calcinated powders was determined to be 0.0145 min^{-1}, which was much larger than the values of 0.00429 min^{-1} and 0.00256 min^{-1}, defined for 350 °C- and 800 °C-calcinated powders, respectively. High temperature calcination resulted in significantly grain growth (**Fig. 6** and **Fig. 8**), which reduced the specific surface area and in turn a poor photocatalytic performance for the 800 °C-calcinated powder. Moreover, the 550 °C-calcinated powder consisted of anatase, rutile and an insignificant amount of srilankite; while the 800 °C-calcinated one consisted of phase pure rutile, the photocatalytic activity of which is demonstrated to be lower than that of anatase.[33] In comparison with the 350 °C-calcinated powders, which are a mixture of anatase and srilankite, the higher photocatalytic activity of the 550 °C-calcinated powders can be attributed to their higher crystallinity and the coexistence of anatase and rutile which exhibits a "mixed crystal effect".[34] It should be noted that, under the same condition, the commercial Degussa P25 titania nanoparticles exhibited a reaction rate constant of 0.0228 min^{-1}, which was significantly larger than the highest value of 0.0145 min^{-1} for the 550 °C-calcinated powders. However, the well dispersion of P25 nanoparticles in the slurry system makes it much harder to recover when compared with the present powders with 3D hierarchical structures.

Conclusions

A hierarchical flower-like nanoarchitecture consisting of protonated pentatitanate $H_2Ti_5O_{11}\cdot 3H_2O$ nanowires were prepared via a facile low temperature template-free route. Controllable transformation from the titanate nanowires to rutile nanorods can be achieved by a subsequent HCl treatment at 80 and 90 °C. The transformation fulfilled through a dissolution precipitation procedure, which was accelerated by an increasing temperature and HCl concentration. The incorporation of rutile nanorods with the layered titanate resulted in an enhanced adsorption capacity towards dye molecules of both rhodamine B and methylene blue in water. When calcinated in air, the protonated pentatitanate was converted to titania, via an intermediate phase of $H_2Ti_4O_9\cdot H_2O$, with the hierarchical structure preserved for up to 800 °C. The 550 °C-calcinated powder, which consisted of anatase, rutile, and trace srilankite, exhibited the best efficiency when utilized to assist photodegradation of rhodamine B in water under UV illumination.

Acknowledgements

This work is funded by Zhejiang Provincial Natural Science Foundation of China under Grant No. LY13E020001.

Notes and references

[a] *State Key Laboratory of Silicon Materials, Key Laboratory of Advanced Materials and Applications for Batteries of Zhejiang Province and Department of Materials Science and Engineering, Zhejiang University, Hangzhou, 310027, P. R. China. Email: msejmw@zju.edu.cn; Fax: +86-571-87953115; Tel: +86-571-87953115*

1. (a) S.W. Liu, J.G. Yu and M. Jaroniec, *J. Am. Chem. Soc.*, 2010, **132**, 11914; (b) X. H. Yang, Z. Li, G. Liu, J. Xing, C. Sun, H. G. Yang and C. Li, *CrystEngComm*, 2011, **13**, 1378.
2. (a) W. Guo, C. Xu, X. Wang, S. Wang, C. Pan, C. Lin and Z. L. Wang, *J. Am. Chem. Soc.*, 2012, **134**, 4437; (b) J.W. Shiu, C.M. Lan, Y.C. Chang, H.P. Wu, W.K. Huang and W.G. Dian, *ACS Nano*, 2012, **6**, 10862.
3. Z. Hong, M. Wei, T. Lan, L. Jiang and G. Cao, *Energy Environ. Sci.*, 2012, **5**, 5408.
4. C. Wang, L. Yin, L. Zhang, Y. Qi, N. Lun and N. Liu, *Langmuir*, 2010, **26**, 12841.
5. K. K. Manga, Y. Zhou, Y. Yan and K. P. Loh, *Adv. Funct. Mater.*, 2009, **19**, 3638.
6. (a) G. Liu, H.G. Yang, X.W. Wang, L.N. Cheng, H.F. Lu, L.Z. Wang, G.Q. Lu and H.M. Cheng, *J. Phys. Chem. C*, 2009, **113**, 21784; (b) G. Wang, H. Wang, Y. Ling, Y. Tang, X. Yang, R. C. Fitzmorris, C. Wang, J. Z. Zhang and Y. Li, *Nano lett.*, 2011, **11**, 3026; (c) N. Roy, Y. Sohn and D. Pradhan, *ACS Nano*, 2013, **7**, 2532.
7. (a) J. G. Yu, Y. R. Su and B. Cheng, *Adv. Funct. Mater.*, 2007, **17**, 1984; (b) L. Liu, H.J. Liu, Y.P. Zhao, Y.Q. Wang, Y.Q. Duan, G.D. Gao, M. Ge and W. Chen, *Environ. Sci. Technol.*, 2008, **42**, 2342.
8. W. Q. Wu, B. X. Lei, H. S. Rao, Y. F. Xu, Y. F. Wang, C. Y. Su and D. B. Kuang, *Scientific reports*, 2013, **3**, Art. No. 1352.
9. W. Q. Wu, H. S. Rao, Y. F. Xu, Y. F. Wang, C. Y. Su and D. B. Kuang, *Scientific reports*, 2013, **3**, Art. No. 1892.
10. Z. Huang, Z. Wang, K. Lv, Y. Zheng and K. Deng, *ACS Appl. Mater. Interfaces*, 2013, **5**, 8663.
11. M. C. Tsai, M. H. Yang, Y. W. Chang, J. K. Tzeng, C. Y. Lee, H. T. Chiu, H. C. Chen and I. N. Lin, *Mater. Chem. Phys.*, 2013, **143**, 60.
12. J.M. Wu, Y.Q. Zhang, H.X. Xue, G.H. Bai, L.L. Lai and M.Z. Tang, *Sci. Adv. Mater.*, 2012, **4**, 719.
13. J.S. Chen, Y.L. Tan, C.M. Li, Y.L. Cheah, D.Y. Luan, S. Madhavi, F.Y. Boey, L.A. Archer and X.W. Lou, *J. Am. Chem. Soc.*, 2010, **132**, 6124.
14. J. Wang, Y. Zhou and Z. Shao, *Electrochim. Acta*, 2013, **97**, 386.
15. K. Fan, T. Peng, J. Chen, X. Zhang and R. Li, *J. Power Sources*, 2013, **222**, 38.
16. F. Shao, J. Sun, L. Gao, S. Yang and J. Luo, *ACS Appl. Mater. Interfaces*, 2011, **3**, 2148.
17. G. Tian, Y. Chen, W. Zhou, K. Pan, C. Tian, X.R. Huang and H. Fu, *CrystEngComm*, 2011, **13**, 2994.
18. L. Xiang, X. Zhao, J. Yin and B. Fan, *J. Mater. Sci.*, 2011, **47**, 1436.
19. J.Y. Liao, B.X. Lei, D.B. Kuang and C.Y. Su, *Energy Environ. Sci.*, 2011, **4**, 4079.
20. (a) X.M. Song, J.M. Wu and M. Yan, *J. Hazard. Mater.*, 2011, **194**, 338; (b) G. Shang, J. Wu, M. Huang, Z. Lan, J. Lin, Q. Liu, M. Zheng, J. Huo and L. Liu, *J. Mater. Chem. A*, 2013, **1**, 9869.
21. (a) J. Yin, X. Zhao, L. Xiang, X. Xia and Z. Zhang, *Soft Matter*, 2009, **5**, 4687; (b) H. Zhang, H. Yu, Y. Han, P. Liu, S. Zhang, P. Wang, Y. Cheng and H. Zhao, *Nano Res.*, 2011, **4**, 938; (c) M. Ye, H. Y. Liu, C. Lin and Z. Lin, *Small*, 2013, **9**, 312.
22. L. Dou, L. Gao, X. Yang and X. Song, *J. Hazard. Mater.*, 2012, **203-204**, 363.
23. J. Sun and J.M. Wu, *Sci. of Adv. Mater.*, 2013, **5**, 549.
24. (a) S.F. Xie, B.J. Zhang, Q. Kuang, X. Wang, Z.X. Xie and L.S. Zheng, *CrystEngComm*, 2012, **14**, 7715; (b) J.Q. Huang, Y.G. Cao, Z.G. Liu, Z.H. Deng and W.C. Wang, *Chem. Eng. J.*, 2012, **191**, 38; (c) B.X. Liu, J.S. Wang, J.S. Wu, H.Y. Li, Z.F. Li, M.L. Zhou and T.Y. Zuo, *J. Mater. Chem. A*, 2013, **2**, 1947.
25. M. Feng, W. You, Z. Wu, Q. Chen and H. Zhan, *ACS Appl. Mater. Interfaces*, 2013, **5**, 12654.
26. T. Sasaki, Y. Komatsu and Y. Fujiki, *Chem. Mater.*, 1992, **4**, 894.
27. N. Mir and M. Salavati-Niasari, *Electrochim. Acta*, 2013, **102**, 274.
28. T. Bezrodna, G. Puchkovska, V. Shymanovska, J. Baran and H. Ratajczak, *J. Mol. Struct.*, 2004, **700**, 175.
29. D. Gong, V. P. Subramaniam, J. G. Highfield, Y. Tang, Y. Lai and Z. Chen, *ACS Catal.*, 2011, **1**, 864.
30. J. Yang, X. Wu, X. Li, Y. Liu, M. Gao, X. Liu, L. Kong and S. Yang, *Appl. Phys. A*, 2011, **105**, 161.
31. M. Sathish, B. Viswanathan and R. P. Viswanath, *Appl. Catal. B: Environ.*, 2007, **74**, 307.
32. J.M. Wu and T.W. Zhang, *J. Photochem. Photobiol. A: Chem.*, 2004, **162**, 171.
33. O. Carp, *Prog. Solid State Chem.*, 2004, **32**, 33.
34. B. Li, J. M. Wu, T. T. Guo, M. Z. Tang and W. Wen, *Nanoscale*, 2014, **6**, 3046.

